

Synchrotron X-ray CT characterization of titanium parts fabricated by additive manufacturing. Part I. Morphology

Nicola Vivienne Yorke Scarlett,^{a*} Peter Tyson,^b Darren Fraser,^c Sheridan Mayo^c and Anton Maksimenko^d

Received 4 January 2016

Accepted 2 May 2016

Edited by A. Momose, Tohoku University, Japan

Keywords: additive manufacturing; titanium; X-ray tomography.

^aMineral Resources, CSIRO, Bayview Avenue, Clayton, Victoria 3168, Australia, ^bInformation Management and Technology, CSIRO, Bayview Avenue, Clayton, Victoria 3168, Australia, ^cManufacturing, CSIRO, Bayview Avenue, Clayton, Victoria 3168, Australia, and ^dImaging and Medical Beamline, Australian Synchrotron, 800 Blackburn Road, Clayton, Victoria 3168, Australia. *Correspondence e-mail: nicola.scarlett@csiro.au

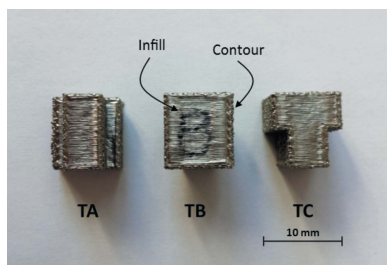
Synchrotron X-ray tomography has been applied to the study of titanium parts fabricated by additive manufacturing (AM). The AM method employed here was the Arcam EBM[®] (electron beam melting) process which uses powdered titanium alloy, Ti64 (Ti alloy with approximately 6%Al and 4%V), as the feed and an electron beam for the sintering/welding. The experiment was conducted on the Imaging and Medical Beamline of the Australian Synchrotron. Samples were chosen to examine the effect of build direction and complexity of design on the surface morphology and final dimensions of the piece.

1. Introduction

Additive manufacturing (AM) technologies such as Arcam's EBM[®] (electron beam melting) system make it possible to manufacture parts with highly complex geometries that would be very difficult to make using traditional manufacturing methods (Wong & Hernandez, 2012). This design freedom provides contemporary product designers with numerous opportunities to optimize the design of a part for performance, free from traditional limitations.

The properties discussed in this paper include external morphology, accuracy of design reproduction and surface area/volume. These may be measured by other techniques but not simultaneously and not without addressing sampling issues. Higher-resolution electron microscopy (EM) examination of external morphology may be achieved but would be limited by the size of the piece, although this is also true to a degree for the synchrotron tomography. Surface area and porosity may be assessed *via* gas adsorption (Sing, 1998) and surface roughness may be determined using profilometry (Stout & Blunt, 2000). Internal morphology and assessment of defects in such pieces will be the subject of Part II (Scarlett *et al.*, 2016) of this publication.

In all cases, the roughness that is characteristic of EBM[®]-made components presents a challenge when a smooth surface finish is desirable. However, this same roughness increases the surface areas of designed pieces, making AM parts very attractive for certain applications. Examples of these include static and micro mixers where a high surface area to volume ratio is desirable for maximum contact between reactants and the acetabular cup (hip implant) and tracking tag for big fish which are discussed in Part II of this work. In the case of the acetabular cup, surface roughness improves bone growth in



the implant and in the fish tag the roughness improves penetration and retention in the fish's skin. Thus the ability to predict and control the surface morphology of AM pieces would be of considerable benefit at both the design and finishing stages.

Assessment of titanium EBM[®] components often focuses on mechanical properties and microstructure (Simonelli *et al.*, 2014; Wauthle *et al.*, 2015). The use of X-ray tomography (Léonard *et al.*, 2012; Tammam-Williams *et al.*, 2015; Van Bael *et al.*, 2011) is relatively uncommon but may bring additional knowledge to these analyses. Such knowledge could contribute to the development and verification of computer models to optimize process conditions and predict material performance and quality (Martukanitz *et al.*, 2014). X-ray tomography has potential benefit for the industry *via* its combination of various qualitative and quantitative measurements from a single non-destructive experiment.

2. Experimental

Arcam Electron Beam Melting¹ (EBM[®]) is an additive manufacturing technology that uses an electron beam to melt and fuse metal powders, layer-by-layer, into three-dimensional parts. The process takes place in a powder bed where a rake feeds a layer of powder over a starting plate on a vertically movable table. In the manufacture of the pieces discussed here the feed material was titanium alloy, Ti64 (Ti alloy with approximately 6% Al and 4% V), with a particle size of approximately 45–106 μm (d_{50} median size of 70 μm). Light sintering of the entire layer and melting of the cross section of the parts in the layer is achieved by electron-beam melting. The table lowers into a tank and the process is repeated. The process is conducted in a vacuum at high bed temperatures during the entire build. A typical starting bed temperature for Ti64 is 730°C. The electron beam used for melting is also used first to heat the start plate.

The exterior of each piece is based on a computer aided design (CAD) model which is translated into STL (Standard Tessellation Language) format which is then used to develop a slice file for the build protocol (Martukanitz *et al.*, 2014). The outer surfaces or contours are formed by a separate melting process from the subsequent cross-hatched infill. The contours are made by stitching many small meltpools together while the hatching is a continuous weld pool.

2.1. Samples

The samples reported here are three solid T-pieces (approximately $1 \times 1 \times 1$ cm) constructed so as to examine the effect of build direction, and a small mesh cube structure (approximately $1 \times 1 \times 1$ cm) which presents fine features and a complex internal shape. The T-pieces were built on the starting plate. No support was used for these pieces as they are

¹The specifics of the process used in the manufacture of these samples are Arcam software process themes 3.2.121; 50 μm layers; melt theme (hatching) speed function 98; two contours inner and outer and offset to contour 0.05 mm.

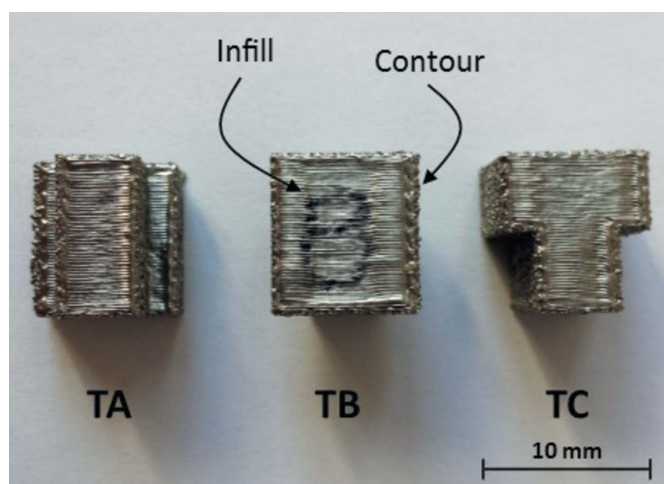


Figure 1
Optical images of the three T-pieces showing different directions of manufacture. The uppermost surface of each as shown is the final, or top, surface of the build. The 'contour' and 'infill' of TB have been labelled.

relatively small and the overhang on one direction of the T-shape was not considered big enough to need support. The cube was built above the plate but again not considered big enough to need support. Fig. 1 shows the T-pieces, with the final surface from the manufacture uppermost. All were manufactured to the same STL file. Fig. 2 shows the mesh cube with its different faces uppermost.

2.2. Synchrotron data collections

Synchrotron radiation was employed in this study due to the size of the pieces and the highly absorbing nature of Ti necessitating the use of high-energy X-rays. The use of a monochromatic beam gives better contrast resolution and obviates artefacts such as beam hardening. The rapid data collection available at synchrotron facilities also allowed a wide range of samples to be examined in a reasonable time-frame.

Experiments were conducted in Hutch 3B of the Imaging and Medical Beamline (IMBL) (Stevenson *et al.*, 2012) at the Australian Synchrotron using the 'Ruby' detector. This is the first of the IMBL detectors to be custom designed. It is based

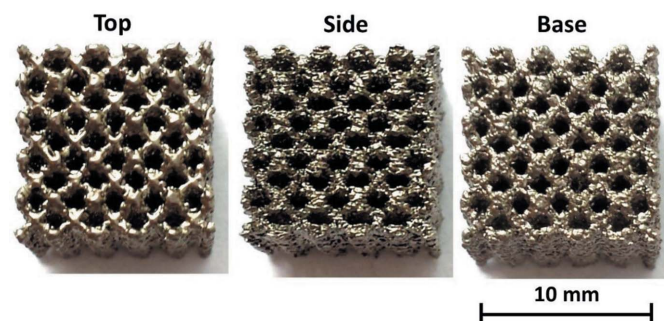


Figure 2
Optical images of the cube sample showing visible variation in surface morphology between the top, side and base.

on the simple concept of a photo-sensitive device coupled by a bright lens to a suitable X-ray sensitive scintillator. The system was conceived by the IMBL team and designed and fabricated at Monash University in the Division of Biological Engineering at the Laboratory for Dynamic Imaging (LDI). The sensor is the PCO.edge mounted on a vertical motor-driven slide set within a light-tight enclosure. A mirror is used to view a phosphor plate set orthogonally to the direction of the beam. This allows protection of the sensor from direct and scattered beam radiation using suitable high-Z materials.

For this experiment the sensor was equipped with a Nikon Micro-Nikkor 105 mm/f 2.8 macro lens allowing the slide to be used as a zoom control. The scintillator was a 12 μm-thick terbium-doped gadolinium oxy-sulfide (Gadox, P43) screen with aluminium powder coat as an optical block. During the experiment the system was tuned to produce 2560 × 2160 images giving a field of view of ~30 × 15 mm with a pixel size of 11.3 μm (note that the actual spatial resolution is typically two to three times this, *i.e.* ~30 μm). Data were collected using monochromatic X-rays of energies 50 and 80 keV for the cube and T-pieces, respectively, in order to ensure reasonable X-ray transmission ($I/I_0 > 20\%$).

The pieces were positioned vertically on the sample stage such that their centre of rotation kept the region of interest within the field of view of the detector. Each tomographic scan was collected over a 180° range in 0.1° steps, making 1800 views in total, with an exposure time of 0.6 s per view.

2.3. Data analysis

For each sample, the 1800 radiographs were reconstructed into orthogonal slices using the *X-TRACT* software (Thompson *et al.*, 2012) on the MASSIVE supercomputer cluster (Goscinski *et al.*, 2014). A ring filter was applied to sinograms prior to reconstruction which reduced, but did not entirely remove, ring artefacts as can be seen in a tomographic slice from one of the T-piece datasets (Fig. 3). The reconstructed slices were then imported as volumes and rendered

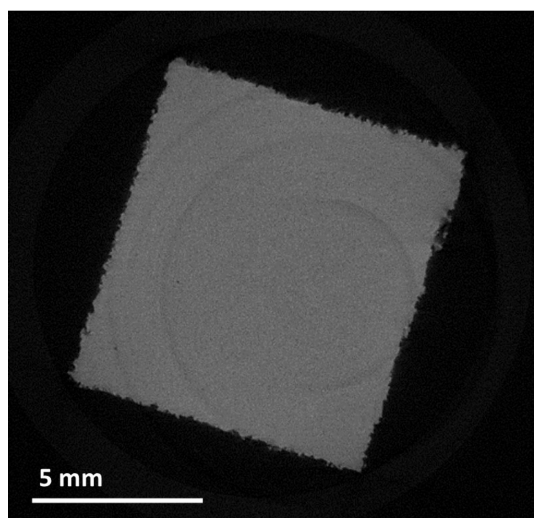


Figure 3
Reconstructed slice from one of the T-piece datasets.

for visualization and measurement using *AvizoFire*® software (Visual Sciences Group). Quantification of surface area and volume were also carried out using *AvizoFire*®.

3. Results and discussion

Tomographic imaging of the samples shows the clear variation in the surface morphology depending upon the design of the piece and the direction of manufacture. The final (upper) surfaces of the pieces are smooth in comparison with the sides and lower surfaces which have well preserved spherical morphologies of the original powder. This is consistent with higher-resolution scanning electron microscope (SEM) images of similar materials (Fig. 4). Slices through the rendered volumes show solid material with very little (less than 1%) porosity (Fig. 3).

3.1. T-pieces

The T-pieces were made and labelled TA, TB and TC as shown in Fig. 1. Those images show clearly the external contour which is made *via* a separate melt from the hatching infill. The upper surfaces of the T-pieces showed a raised ‘scalloped’ edge (the contour) and a depression in the central region of the infill. This is most obvious in TB which has the largest upper surface (Fig. 5). The depression in the centre of the face may relate to the contour layer being made first and then filled in. It appears that the contour holds up the edges of the infill but is insufficient to support the central region which effectively ‘sags’ as it cools. The infill requires variable speed of the beam across the width of the sample. Its speed is faster in the middle but it then has to turn around at the edges causing a heat trail to overheat this area. The faster the beam, the less time the material stays at temperature and molten which may produce more shrinkage in the middle. Typically, a turning point function tries to compensate by increasing speed around the edges but may need more adjustment in this case. The layer thickness in the depression appears narrower and more variable than it does closer to the edges which may also relate to this more rapid cooling. Adjustment to the focus offset may help in this case making the weld pool shallower. The scalloped edges may result from the turn point in the

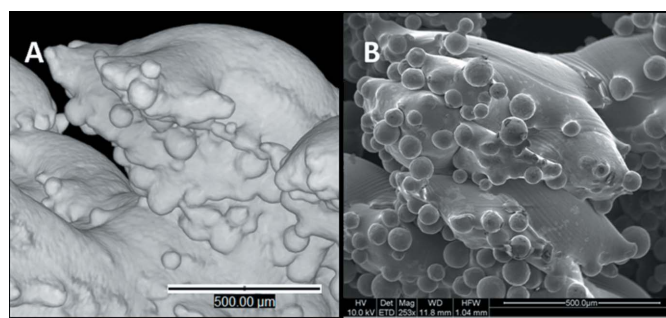


Figure 4
(A) Tomographic image and (B) SEM image of similar AM fabricated meshes.

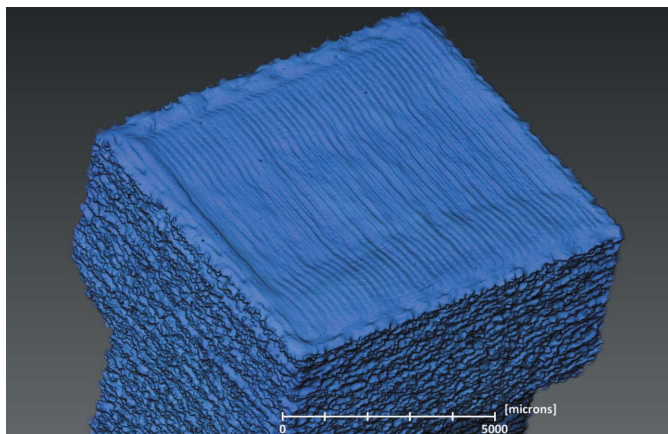


Figure 5
Upper surface of TB showing morphology typical of the final layer of manufacture.

hatching being consistently offset with respect to the contour. This can be seen in Fig. 5 where the final layer of hatching seems to fall short of the upper edge in the image. A similar effect is seen on the left-hand side in the image. This suggests that a similar offset is occurring in the orthogonal layer of hatching immediately below the surface layer which has resulted in the near edge being raised with respect to the face and showing the surface morphology of the contour rather than that of the hatching. Generally the contouring is used to give a better surface finish and the hatching should not penetrate past the contour.

This edge effect is very pronounced on the upper surface of TA where the final surface faces are narrower than that of TB (Fig. 6). In this sample the hatching appears to have reached further into the width of the contour at the lower edges (in the image) on both the top of the piece and its ledge than on the upper edges (in the image). The upper edges are appreciably more ragged than the lower and suggest variability in the

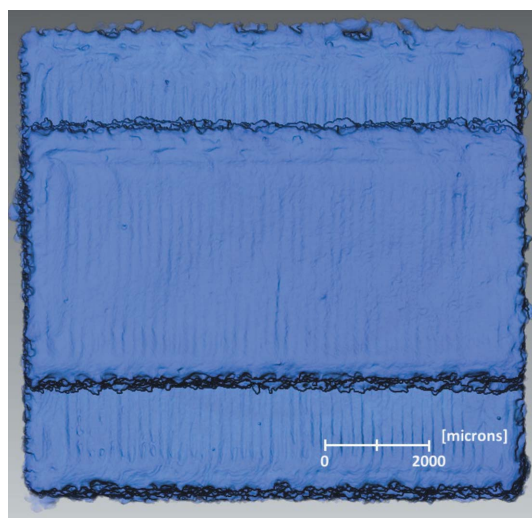


Figure 6
Upper surface of TA showing morphology typical of the final layer of manufacture.

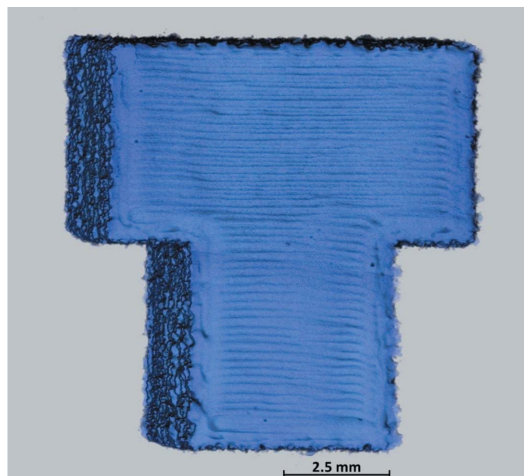


Figure 7
Upper surface of TC showing morphology typical of the final layer of manufacture.

interfaces between each layer of hatching and the contour. The outer edge of the upper ledge in the image is particularly uneven and there appears to have been appreciable interaction between the contour and the hatching. There also looks to have been considerable deviation from the ends of the lines of the hatching and possibly increased melting at the interface with the contour. These results suggest that adjusting parameters such as offset to contour should be considered to avoid hatching penetrating too much into the contour.

The final surface of TC exhibits similar features to TA and TB but there appears to be greater variability in the layer thickness of its infill (Fig. 7). The depression apparent in the top surfaces of TA and TB is also apparent here but is thinner and offset to the right (in the image) in the narrower part of the face.

All the final faces show a small number of craters of approximately 100–200 μm which have the appearance of gas porosity, although that is frequently smaller than this (*i.e.* 10–50 μm). The individual layers of the contours around the sides of the T-pieces are generally all similar in appearance with a thickness of approximately 200 μm . This is difficult to measure as the layers are very uneven which is partially due to the retained powder morphology at the bottom of each.

The morphology and design accuracy of the ledges between the horizontal and vertical parts of the T-pieces are highly dependent on the build direction as shown in Fig. 8. TA and TC show approximate right angles at their corners while TB has angles clearly greater than 90°. The outer corners and surface morphology of the ledges also vary with build direction. Although TA and TC have right angles, the final-layer surface morphology of TA means that there is overhang of material as described above and a slight depression in the face of the ledge (Fig. 8). The ledges of TC are flat and the outer corners have clear right angles as it is made up of layers of the external contours. In TB these ledges have been manufactured as overhangs (*i.e.* unsupported) and, as well as showing strong deviation from right angles on their inner corners, their faces

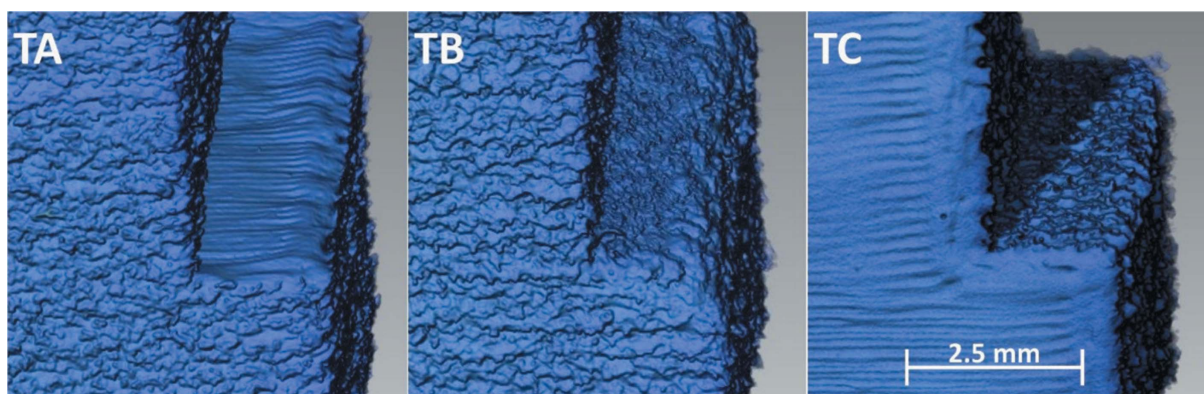


Figure 8
Comparison of ledge morphologies of the three T-pieces.

are very sloped and rounded at their outer edges. The surface morphology of these ledges is very porous and uneven which is consistent with being built as an overhanging face where the electron beam is scanning on loose powder with no supporting material. The finish on TB's ledges also varies from one side of the piece to the other.

3.2. Cube

The cube (Figs. 2 and 9) is a complex shape which is essentially a three-dimensional mesh. The final surface has the smooth appearance associated with the finish of a build. The sides of the piece as manufactured have the expected rough finish but the retained powder morphology is less well defined than that observed in the T-pieces. In contrast with other samples, however, the bottom surface has a similarly smooth appearance to the top (Fig. 10) although the final surface is visibly shinier and has a smoother feeling to the touch (Fig. 2).

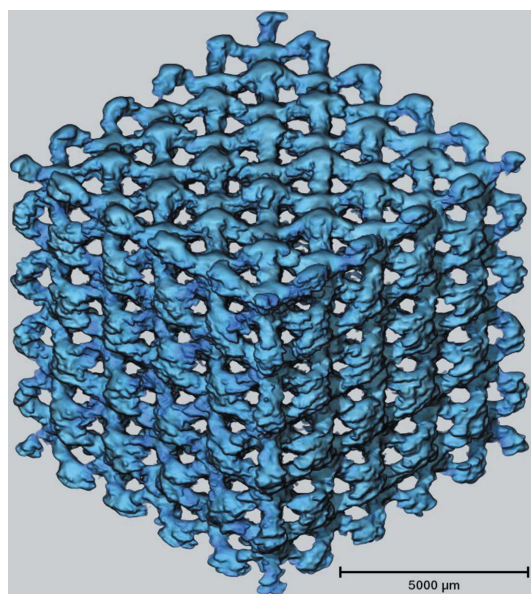


Figure 9
The three-dimensional mesh of the cube sample with the final surface uppermost.

This rounding of the base results from the piece being manufactured directly from the powder bed rather than on a substrate like the T-pieces. The view in Fig. 10 also shows where material has bridged the designed holes in the piece and been retained.

3.3. Quantitative analysis

3.3.1. Surface area and volume. Surface areas and volumes have been calculated using *AvizoFire*[®]. It is important to note that the reconstruction step of the data analysis has considerable impact on these calculations and that the values should therefore be regarded as semi-quantitative. Filtering of the original data in any way to remove noise produces a smoother surface and consequently reduces the surface area. Conversely, any error in the centre of rotation used for the reconstructions is likely to introduce artefacts which increase the measured surface area. The process of reconstruction is therefore not absolute and consideration must be given to the fact that it remains somewhat operator dependent. Visual

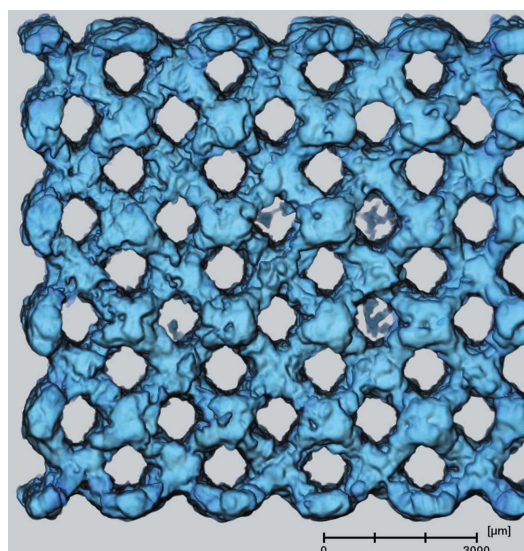


Figure 10
The base of the cube sample showing rounded surface morphology.

inspection of the reconstructed slices was carried out to minimize the likelihood of such artefacts remaining in the data used here. The data were also processed under identical conditions to make the results comparable and internally consistent.

Fig. 11 shows reconstructed slices and renderings from the cube sample. Panel A shows a reconstructed slice based on raw data, and panel D shows the same using smoothed data. Volume renders of these reconstructions are shown in panels B and E, respectively. Visually either treatment appears reasonable, but, while the volumes of the two are similar ($\sim 320 \text{ mm}^3$), the surface areas differ greatly. The surface area in panel B is of the order of 4400 mm^2 while that in panel E is around 2500 mm^2 . Consequently the surface area-to-volume ratios (SA/vol) differ by a factor of almost two. Another possible source of variation is the use of filtering at the rendering stage in order to improve the appearance of noisy data. An example of this is shown in panel C of Fig. 11. In this case the surface area is around 3000 mm^2 giving a SA/vol value somewhere between the others. Inspection of optical images (panel F in Fig. 11) shows that the surface appearance is similar to that shown in panel B. Without this confirmation, however, such a finish may be erroneously dismissed as noise.

Accurate reproduction of the design is important for any manufacturing process. In order to assess this, measurements of the AM pieces were compared with those of the relevant

Table 1

Semi-quantitative analysis of surface areas and volumes from selected samples.

The numbers in brackets represent the factor by which the fabricated piece deviates from the design.

| Sample | Surface area (mm^2) | Volume (mm^3) | SA/vol (mm^{-1}) |
|-------------|--------------------------------|--------------------------|-----------------------------|
| TA | 865 (1.7) | 601 (0.9) | 1.4 (2.0) |
| TB | 1065 (2.0) | 615 (0.9) | 1.7 (2.4) |
| TC | 927 (1.8) | 611 (0.9) | 1.5 (2.1) |
| T design | 520 | 700 | 0.7 |
| Cube | 5000 (1.9) | 320 (0.6) | 15.6 (2.9) |
| Cube design | 2646 | 503 | 5.3 |

STL files. SA/vol calculations have been made and the models and designs have been overlaid in order to examine areas of difference.

Table 1 shows the results of surface area and volume analysis. In general, the volumes of the manufactured pieces were smaller than those of the designs mainly through shrinkage of the pieces on cooling.

The T-pieces all increased their surface area from design by a factor of about two primarily due to the surface finish inherent in this manufacturing process. The volumes shrunk to approximately 90% of the design and the consequential change in SA/vol was around a twofold increase. A far greater change was observed in the cube. The change in surface area

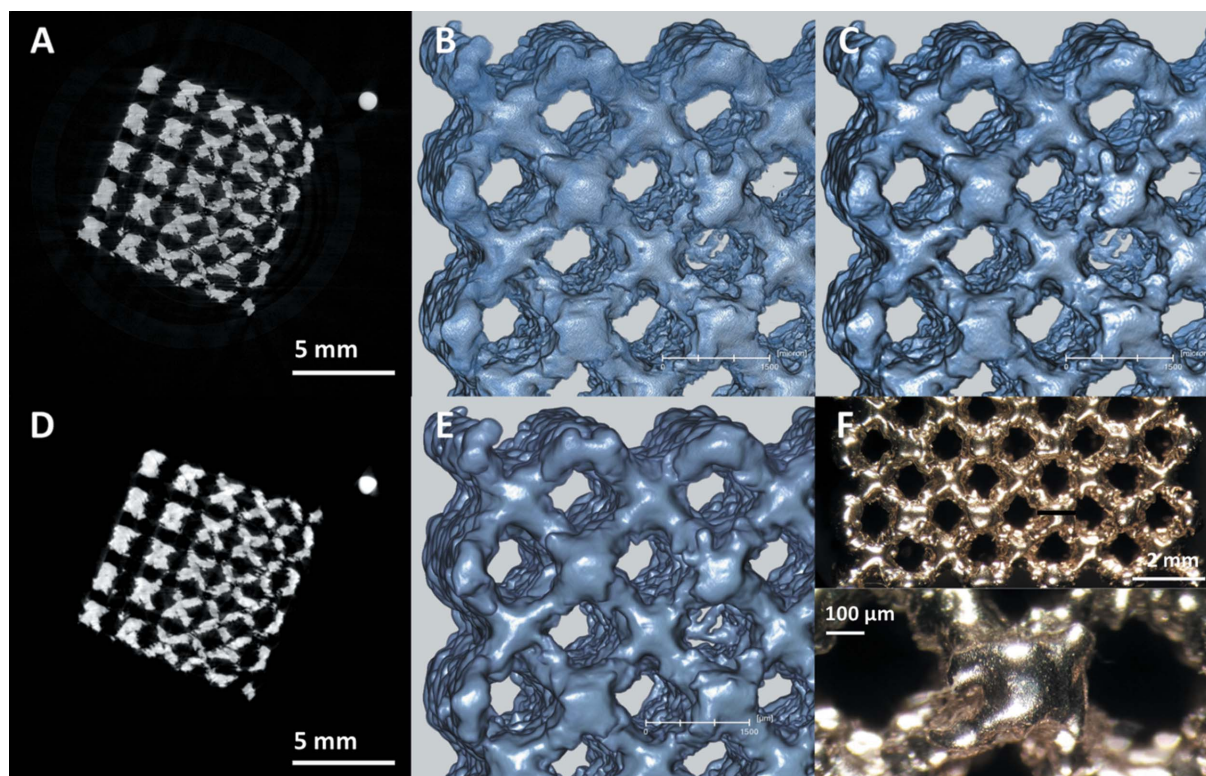


Figure 11
Comparison of results from raw and filtered data. Panel A shows a reconstructed slice from raw data; panel B shows a rendering of the raw data shown in panel A; panel C shows a rendering of the data shown in panel A following a median filter; panel D shows a reconstruction using a small degree of phase extraction as a means of smoothing; panel E shows a reconstruction of the raw data shown in panel D; and panel F shows optical images of the actual piece.

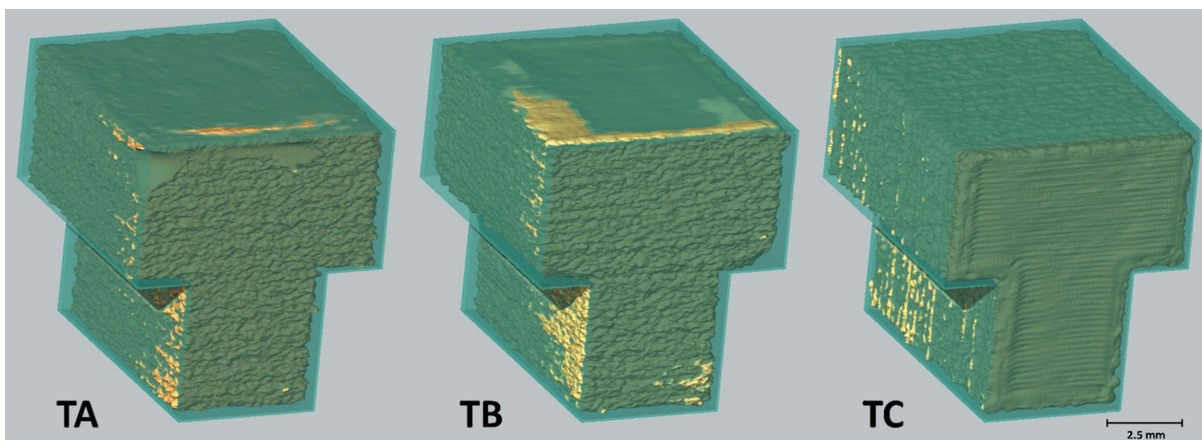


Figure 12
Comparison of T-piece models with surface generated from CAD file.

from design to model is similar to that of the T-pieces, *i.e.* approximately twofold, but the volume of the model is reduced to about 60% of the design. This combines to produce an almost threefold increase in SA/vol.

3.3.2. Accuracy of design reproduction. The rendered volumes from the CT measurements and those generated directly from the STL files have been aligned to look for where any differences between the design and the product have occurred. The greatest difference is due to the roughening of the surface which is a function of the AM process but there are issues of asymmetry and shrinkage which are also apparent.

AvizoFire[®] computes an affine transformation to align two triangulated surfaces generated from (i) the tomographic data and (ii) the STL file. Following this alignment process, a transparent rendering of the surface from the STL file can then be visualized as an overlay on that of the model.

T-pieces. Fig. 12 shows surfaces generated from the tomographic scans of the T-piece models overlaid by a transparent rendering of that generated from the STL file. The surfaces have been aligned as described above. (A set of reference coordinates is shown in Fig. 13.)

In general the models fall within the design outline but there are regions of deviation. TA is built from F to E according to the scheme shown in Fig. 13. TB is built the other way up, *i.e.* from E to F. Both of these show greater deviation from the model than does TC which is built from A to B. TA and TB appear to have shrunk from the design slightly unevenly and as a consequence do not sit squarely within the design envelope.

TC is generally well aligned with the design. The shrinkage is more uniform than that of TA and TB. The only protrusions that may be seen are regular lines along the sides of the piece corresponding to the layers of manufacture. This is consistent with the roughening of the surface finish *via* the retention of powder morphology along the edges of the piece. This ‘striped’ deviation is also visible in places on TA and TB.

Both TA and TB are built such that the outer contour of the piece changes in shape as the build progresses. In the case of TA there is a sharp change from a square to a narrow

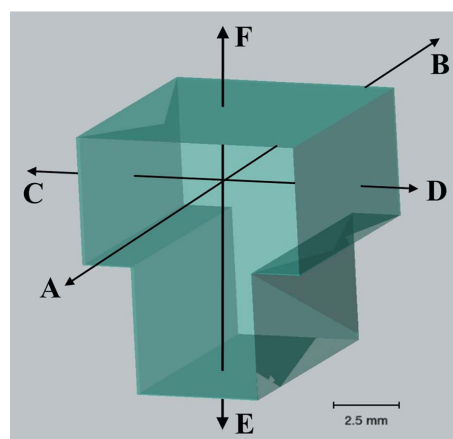


Figure 13
Labelling scheme for directions within the T-piece design.

rectangular contour about half way up the build. The reverse is true for TB. TB exhibits clear mismatch with the design at the point of transition between the contours. This is to be expected given the morphology of the overhanging portions as described in §3.1. The outer contour of TC is constant throughout the build and has produced a model which is more faithful to the design than the others.

Cube. Fig. 14 shows a surface generated from the tomographic scan of the cube model overlaid by a transparent rendering of that generated from the STL file. The surfaces have been aligned as described above. In general the model falls within the design outline but there are regions where it protrudes outside the design boundary. The bottom of the model shows deviation where the piece has been fabricated directly from the powder bed and one of the sides has protrusions in keeping with the surface roughness characteristic of AM.

As reported in §3.3.1 and Table 1, the volume of the cube model is significantly less than that of the design (~60%). Whilst there is slight overall shrinkage of the piece the main source of this difference is in the thickness of the ‘arms’ which

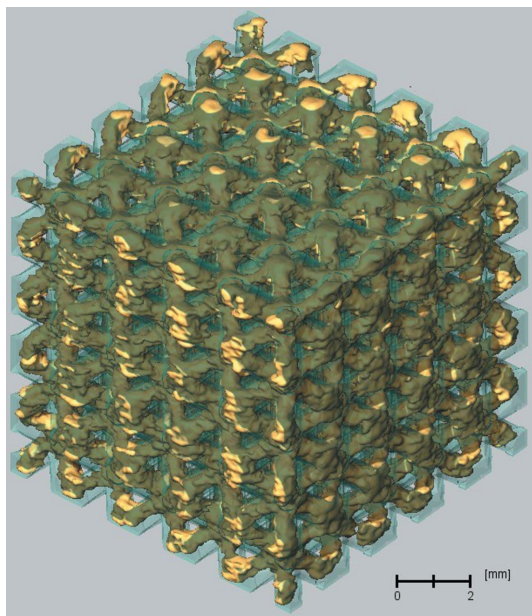


Figure 14
Comparison of cube model with surface generated from CAD file.

comprise the mesh. This can be clearly seen in Fig. 15. This reduction in diameter is partially attributable to the fact that, in effect, all the arms are manufactured as unsupported overhangs with the associated problems described above (§3.1). There is also the issue of the manufacturing process being unable to accurately produce a smooth, roughly cylindrical section of such small dimensions. The diameter and shape of the section is limited by the size of the powder feed material and the consequent thickness of the layers.

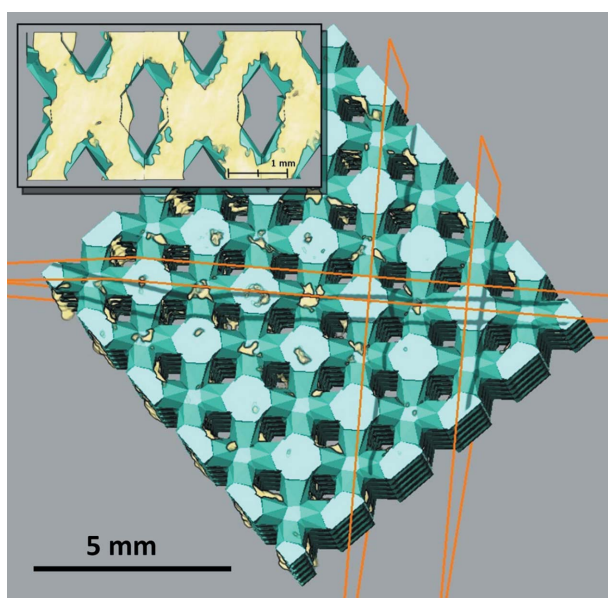


Figure 15
Portion of a single layer of cube model (inset) overlaid with the corresponding surface generated from the CAD file. The clip planes used to define the layer are shown in orange on the image of the full model.

4. Conclusion

The aim of this experiment was to use X-ray tomography to characterize some of the physical properties of titanium parts fabricated by additive manufacturing (AM). The major findings of this study relate to the accuracy with which the build reproduces the design, the effect of the AM process on surface finish and the influence of the build protocol.

The surface finish of the pieces was greatly influenced by the size and the direction of build. The sides of the contours had clearly retained powder morphology where the final surfaces of the hatching were relatively smooth. Differences in the final surfaces of the pieces appear to result from variable heating and cooling rates dictated by the build strategy.

The study here showed clearly that accuracy of reproduction was also affected by the direction in which the part was built relative to its design. Solid T-pieces which had been built in different directions demonstrated this relationship well. Where the outer contour of the piece changed during the build (*i.e.* when the T was built from either the top down or the bottom up), the reproduction of the design was less faithful than where the contour was consistent throughout the build (*i.e.* when the T was built from front to back).

The small mesh cube demonstrated the limitations regarding the reproduction of the small-diameter linking rods of the mesh. Such small-diameter sections were significantly affected by the magnitude of the surface roughness relative to the absolute dimension. In this example the rods of the model were generally thinner than the design and as a consequence the overall volume of the piece was reduced to 60% of the planned volume.

X-ray tomography has proved to be useful in the characterization of AM pieces in the provision of data which allows a range of simultaneous qualitative and quantitative measurements. It is anticipated that such findings will bring greater understanding of the interplay between design (size and shape) and build parameters (direction, support structure, *etc.*). Such understanding may be employed in improved build algorithms and process modeling thus contributing to prediction and non-destructive assessment of structure–property relationships.

Acknowledgements

This research was undertaken on the Imaging and Medical Beamline (IMBL) at the Australian Synchrotron, Victoria, Australia. The authors wish to acknowledge the assistance of Dr Andrew Stevenson in preparation for the experiment and Mr Ian Madsen and Dr Helen Brand for their assistance during the experiment.

References

- Goscinski, W. J., McIntosh, P., Felzmann, U., Maksimenko, A., Hall, C. J., Gureyev, T., Thompson, D., Janke, A., Galloway, G., Killeen, N. E. B., Raniga, P., Kaluza, O., Ng, A., Poudel, G., Barnes, D. G., Nguyen, T., Bonnington, P. & Egan, G. F. (2014). *Front. Neuroinform.* **8**, 30.

- Léonard, F., Tammas-Williams, S., Prangnell, P. B., Todd, I. & Withers, P. J. (2012). *Conference on Industrial Computed Tomography (ICT) 2012*, Wels, Austria, pp. 85–93.
- Martukanitz, R., Michelaris, P., Palmer, T., DebRoy, T., Liu, Z.-K., Otis, R., Heo, T. W. & Chen, L.-Q. (2014). *Addit. Manuf.* **1–4**, 52–63.
- Scarlett, N. V. Y., Tyson, P., Fraser, D., Mayo, S. & Maksimenko, A. (2016). *J. Synchrotron Rad.* **23**, 1015–1023.
- Simonelli, M., Tse, Y. Y. & Tuck, C. (2014). *Mater. Sci. Eng. A*, **616**, 1–11.
- Sing, K. S. W. (1998). *Adv. Colloid Interface Sci.* **76–77**, 3–11.
- Stevenson, A. W., Hall, C. J., Mayo, S. C., Häusermann, D., Maksimenko, A., Gureyev, T. E., Nesterets, Y. I., Wilkins, S. W. & Lewis, R. A. (2012). *J. Synchrotron Rad.* **19**, 728–750.
- Stout, K. J. & Blunt, L. (2000). *Three-Dimensional Surface Topography*. London: Penton Press.
- Tammas-Williams, S., Zhao, H., Léonard, F., Derguti, F., Todd, I. & Prangnell, P. B. (2015). *Mater. Charact.* **102**, 47–61.
- Thompson, D., Khassapov, A., Nesterets, Y., Gureyev, T. & Taylor, J. (2012). *2012 IEEE 8th International Conference on E-Science (E-Science)*, Chicago, IL, USA.
- Van Bael, S., Kerckhofs, G., Moesen, M., Pyka, G., Schrooten, J. & Kruth, J. P. (2011). *Mater. Sci. Eng. A*, **528**, 7423–7431.
- Wauthle, R., Vrancken, B., Beynaerts, B., Jorissen, K., Schrooten, J., Kruth, J.-P. & Van Humbeek, J. (2015). *Addit. Manuf.* **5**, 77–84.
- Wong, K. V. & Hernandez, A. (2012). *A Review of Additive Manufacturing*. ISRN Mechanical Engineering.